A Fast Algorithm and Practical Considerations for Passive Macromodeling of Measured/Simulated Data

Dharmendra Saraswat, *Student Member, IEEE*, Ramachandra Achar, *Member, IEEE*, and Michel S. Nakhla, *Fellow, IEEE*

***Abstract*—Passive macromodeling of high-speed package and interconnect modules characterized by measured/simulated data has generated immense interest during the recent years. This paper presents an efficient algorithm for transient simulation of interconnect networks characterized by measured/simulated data in the presence of other linear and nonlinear devices. A new set of linear constraints are proposed, which help in preserving the passivity of resulting macromodels. Examples are presented to demonstrate the validity and efficiency of the proposed algorithm.**

***Index Terms*—Algebraic riccati equation, circuit simulation, Hamiltonian matrix, high-speed interconnects, measurements, passive macromodels, S parameters, tabulated data, transient analysis, transmission lines, Y parameters.**

I. Introduction

THE RECENT trend in the very large scale integration (VLSI) industry toward miniature designs, low power consumption, and increased integration of analog circuits with digital blocks has made the signal integrity analysis a challenging task. The ever-increasing quest for high-speed applications has highlighted the previously negligible effects of interconnects, such as ringing, delay, distortion, reflections and crosstalk. It is to be noted that, predicting these effects in high-speed designs is not an easy task, as high-frequency interconnect models become necessary [1]–[26].

However, with the increasing frequency and complexity, it is not always possible to find an analytical model for interconnect network. For instance, interconnects in chip packages are usually nonuniform due to high circuit density, complex shapes and geometrical constraints at the edges of the chip. Numerous similar situations can be found, such as vias, nonuniform transmission lines, on-chip passive components and high-frequency microwave devices, where the interconnect modeling becomes a difficult task. In such cases, the behavior of these devices is generally characterized by sampled data, obtained either directly from measurements or from rigorous full-wave electromagnetic simulations [6]–[22]. The measured/simulated (*tabulated*) data can be in the form of scattering (S), admittance (Y), impedance (Z) or hybrid (H) parameters. As a result, characterization and simulation of interconnect networks based on tabulated data within nonlinear simulation environment is becoming a topic of intense research.

Manuscript received October 23, 2002; revised November 16, 2003.

The authors are with the Department of Electronics, Carleton University, Ottawa, ON K1S 5B6, Canada (e-mail: achar@doe.carleton.ca).

Digital Object Identifier 10.1109/TADVP.2004.825477

However, transient simulation of such frequency-dependent tabulated data in the presence of nonlinear devices is not a straight-forward process. This can be attributed to the mixed frequency/time problem as the network consists of measured subnetwork described by frequency-dependent data and nonlinear devices which are described only in the time-domain. In addition, discrete measured data does not have adequate representation for simulation purposes. More recent approaches to address the above issue are based on obtaining a reduced-order model [9]–[21] for the frequency sampled data and performing transient analysis either by using recursive convolution [23] or by converting the frequency-domain reduced model into a set of ordinary differential equations [1]. However, there are two main difficulties associated with this category of approaches.

1) They suffer from the problem of ill-conditioning in capturing the broadband frequency spectrum of the device.
2) Passivity of the resulting macromodel is not guaranteed.

It is to be noted that, passivity is an important requirement for macromodels. If the macromodel is not passive, then the transient simulation of such macromodels with the rest of the circuitry may suffer from spurious oscillations [1], [25]–[27] (*details in* Section II). Conventional approaches in the literature on imposing macromodel passivity constraints lead to nonlinear optimization formulation, which can be CPU expensive [28]. Alternative approaches use constraints such as, every first or second-order pole-residue pair must strictly conform to passivity relations. However, these constraints are sufficient but not necessary [18] (most practical circuits do not obey these conditions), strict enforcement of these conditions may lead to convergence problems, inaccurate and CPU expensive macromodels. Algorithms such as the ones based on convex optimization [21] can guarantee the passivity of the macromodel. However, they can be CPU expensive, since the associated computational complexity is in the range of n^5 *to* n^6 (where n is the order of the state-space matrix). On the other hand, approaches such as the ones in [9]–[16] are computationally fast. However, they may not strictly guarantee the macromodel passivity and may lead to passivity violations. Hence for such class of algorithms it becomes essential to verify the macromodel passivity and correct for any passivity violations. However, one of the key requirement of these algorithms is the quality of the macromodel prior to post-processing, that is, the extent of their conforming to passivity conditions. Post-processing can be quite effective if the passivity violation is minor; on the other hand, if the violation is significant, it can lead to inaccurate/nonpassive macromodels.

In order to address the above problem, a new algorithm is presented in this paper to efficiently synthesize passive macromodels for measured/simulated data, which keeps the need for post passivity compensation to the minimum. The algorithm mainly involves three steps. In the first step, a multiport vector-fit-based rational approximation [12] is performed to obtain an accurate set of poles. Next, multiport residues are obtained subject to a new set of passivity conforming linear constraints (the associated computational complexity is in the range of n^3). In the last step, a check for any passivity violation is performed using Hamiltonian matrix formulation of the state-space equations obtained from the pole-residue model [30]. For this purpose, two theorems are presented in this paper. In case of passivity violation, necessary compensation is carried out [31], [32].

The rest of the paper is organized as follows. Section II presents the problem formulation. Section III presents a technique to compute accurate poles of the system. Section IV presents the proposed passivity conforming linear constraints and the new residue computation algorithm. Section V describes the passivity check and compensation. Sections VI and VII present computational results and conclusions, respectively.

II. Problem Formulation

The tabulated data can be multiport scattering ($\boldsymbol{S}$), admittance ($\boldsymbol{Y}$), impedance ($\boldsymbol{Z}$), transmission ($\boldsymbol{T}$) or hybrid ($\boldsymbol{H}$) parameters. For the ease of presentation, in this paper it is assumed that the frequency-domain Y-parameter data is given. The admittance matrix of a M-port subnetwork can be written in terms of a rational approximation as

$$\boldsymbol{Y}(s) = [Y_{ij}(s)]; \quad (i,j \in 1 \ldots M);$$
$$Y_{ij}(s) = \frac{\left(a_0^{(i,j)} + a_1^{(i,j)} s + \cdots + a_L^{(i,j)} s^L\right)}{\left(b_0^{(i,j)} + b_1^{(i,j)} s + \cdots + b_N^{(i,j)} s^N\right)}. \tag{1}$$

In the conventional curve fitting methods, (1) is formulated as a linear problem, $\boldsymbol{AX} = \boldsymbol{b}$, where $\boldsymbol{X}$ is the vector of unknown coefficients, $[a_0, \ldots a_L; b_0, \ldots b_N]$. However, this formulation is ill-conditioned [12]. Also the total number of poles in the admittance matrix $\boldsymbol{Y}(s)$ could be too many, which could lead to inefficient simulation.

In addition, the above conventional approach doesn't guarantee passivity of the multiport macromodel. However, the loss of macromodel passivity can be a serious problem because transient simulations may encounter artificial oscillations.

This is because macromodels that are only stable but not passive, can produce unstable networks when connected to other passive loads. On the other hand, a passive macromodel, when terminated with any arbitrary passive load always guarantees the stability of the overall resulting network. To illustrate the point, consider a single-port second-order macromodel shown in Fig. 1(a). The macromodel is stable but not passive. When this macromodel is terminated with the passive load [Fig. 1(b)], the overall network becomes unstable.

Therefore the challenge here is to ensure passivity (in addition to accuracy) of the multiport macromodel. A network with admittance matrix $\boldsymbol{Y}(s)$ is passive [27], iff

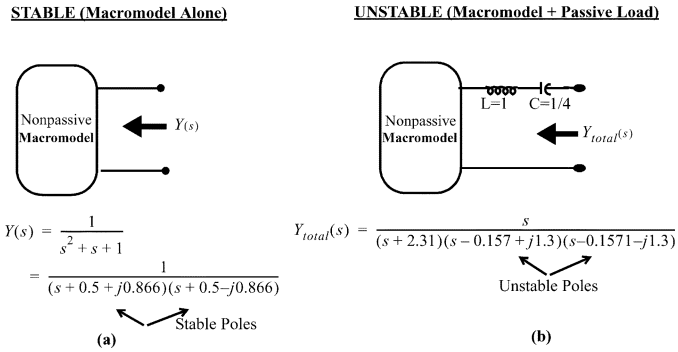

Fig. 1. Illustration of significance of passivity.

a) $\boldsymbol{Y}(s^*) = \boldsymbol{Y}^*(s)$, where '*' is the complex conjugate operator;
b) $\boldsymbol{Y}(s)$ is a positive real (PR) matrix, i.e., the product $\boldsymbol{z}^{*t}[\boldsymbol{Y}^t(s^*) + \boldsymbol{Y}(s)]\boldsymbol{z} \geq 0$ for all complex values of s with $Re(s) > 0$ and any arbitrary vector $\boldsymbol{z}$.

Condition (a) is automatically satisfied since the complex poles/residues of the transfer function are always considered along with their conjugates, leading to only real coefficients in rational functions of $\boldsymbol{Y}(s)$. However, ensuring condition (b) is not easy. For the practical case of networks with symmetric admittance matrices, condition (b) implies that

$$Real(\boldsymbol{Y}(s)) = \frac{\left[\boldsymbol{Y}^t(s^*) + \mathbf{Y}(s)\right]}{2} \tag{2}$$

must be positive definite for all s with $Re(s) > 0$. From [27], if matrix rational function $\boldsymbol{Y}(s)$ has no poles on the closed right-half plane, it is positive real iff

$$Real(\boldsymbol{Y}(j\omega)) = \boldsymbol{F}(j\omega) = \frac{\left[\boldsymbol{Y}^t(j\omega^*) + \boldsymbol{Y}(j\omega)\right]}{2} \geq 0, \quad \text{for } \omega \in \Re \cup \infty. \tag{3}$$

As is obvious from the introduction, ensuring (3) could be a daunting task for macromodels from tabulated data. In this paper, a new algorithm is presented to ensure passivity of macromodels obtained from tabulated data and is based on CPU efficient linear formulation. The algorithm has the following three steps. In the first step, a multiport vector-fit-based rational approximation [12] is performed to obtain a good set of poles (details in Section III). Next, multiport residues are obtained subject to new passivity conforming linear constraints (details in Section IV). In the last step, a check for any passivity violation is performed using Hamiltonian matrix formulation [37] of state-space equations and if necessary, the macromodel is compensated for any passivity violation (details in Section V).

III. Computation of Multiport Dominant Pole-Set (Step 1)

This step computes an accurate pole-set for the given multiport admittance matrix. For this purpose, the pole identification algorithm of the vector fitting approach [12] is extended to efficiently handle the case of multiport networks. Here, an initial guess of poles is considered and a scaling function is introduced.

With this initial guess of poles the scaled function is fitted, from which an accurate set of poles are computed. However, finding pole-sets individually for each element of the admittance matrix can lead to large number of redundant poles in the macromodel resulting in inefficient transient simulation. Also, identifying a common multiport pole-set from pole-sets of individual elements of the admittance matrix is generally heuristic and can lead to errors. In order to overcome the above problem and to minimize the number of poles in the matrix-transfer function, the following two propositions are used [11].

1) In general, the pole set corresponding to any individual element of the admittance matrix is a subset of the union of all driving point admittances [33].
2) Generally, in a system with large number of dominant poles, pole sets belonging to different driving point admittances contain mostly identical poles and only a very small percentage of poles differ among these sets.

Using the above two propositions, a common pole-set for the multiport pole-residue model is obtained by performing the *pole identification algorithm* of the vector fitting approach [12] on driving point admittances. This is done as follows. The admittance matrix of a M-port electrical network can be written as

$$\boldsymbol{Y}(s) = \begin{bmatrix} Y_{11}(s) & Y_{12}(s) & \dots & Y_{1M}(s) \\ \vdots & \vdots & \ddots & \vdots \\ Y_{M1}(s) & Y_{M2}(s) & \dots & Y_{MM}(s) \end{bmatrix}. \quad (4)$$

To obtain a common pole-set, vector-fitting algorithm is carried out on the vector of the diagonal entries of the admittance matrix (proposition 1). For the case of M-port network of (4), the vector

$$\boldsymbol{Y}_{\text{diag}}(s) = \begin{bmatrix} Y_{11}(s) \\ Y_{22}(s) \\ \vdots \\ Y_{MM}(s) \end{bmatrix} \quad (5)$$

is fitted. Each element of (5) is approximated with the following pole-residue formulation:

$$Y_{ii}(s) = \sum_{n=1}^{N} \frac{k_n^{i,i}}{s - p_n} + c^{i,i} + sh^{i,i} \quad (6)$$

where the residues (k_n) and poles (p_n) can be real or complex conjugate pairs, N is the number of poles and residues, c and h are real constants. Next, an initial guess of pole-set $\bar{\boldsymbol{P}} = (\bar{p}_1, \bar{p}_2, \dots \bar{p}_N)$ is specified and a scaling function $\sigma(s)$ of the following rational form is considered:

$$\sigma(s) = \sum_{n=1}^{N} \frac{\tilde{k}_n}{s - \bar{p}_n} + 1. \quad (7)$$

Next, $\boldsymbol{Y}_{\text{diag}}(s)$ of (5) is multiplied by the above scaling function and the scaled function $(\sigma \boldsymbol{Y}_{\text{diag}})(s)$ can be expressed as

$$(\sigma \boldsymbol{Y}_{\text{diag}})(s) = \begin{bmatrix} (\sigma Y_{11})(s) \\ \vdots \\ (\sigma Y_{MM})(s) \end{bmatrix}$$

$$= \begin{bmatrix} \sum_{n=1}^{N} \frac{\hat{k}_n^{11}}{s - \bar{p}_n} + \hat{c}^{11} + s\hat{h}^{11} \\ \vdots \\ \sum_{n=1}^{N} \frac{\hat{k}_n^{MM}}{s - \bar{p}_n} + \hat{c}^{MM} + s\hat{h}^{MM} \end{bmatrix}. \quad (8)$$

Next, multiplying (7) by $\boldsymbol{Y}_{\text{diag}}(s)$ and then equating it to (8), we can write

$$(\sigma \boldsymbol{Y}_{\text{diag}})(s) \approx \sigma(s) \boldsymbol{Y}_{\text{diag}}(s) \quad (9)$$

or, from (5)

$$\begin{bmatrix} (\sigma Y_{11})(s) \\ \vdots \\ (\sigma Y_{MM})(s) \end{bmatrix} \approx \begin{bmatrix} \sigma(s) Y_{11}(s) \\ \vdots \\ \sigma(s) Y_{MM}(s) \end{bmatrix}. \quad (10)$$

Using (7) and (8), we can write (10) as

$$\begin{bmatrix} \sum_{n=1}^{N} \frac{\hat{k}_n^{11}}{s - \bar{p}_n} + \hat{c}^{11} + s\hat{h}^{11} \\ \vdots \\ \sum_{n=1}^{N} \frac{\hat{k}_n^{MM}}{s - \bar{p}_n} + \hat{c}^{MM} + s\hat{h}^{MM} \end{bmatrix} - \begin{bmatrix} \left(\sum_{n=1}^{N} \frac{\tilde{k}_n}{s - \bar{p}_n} \right) Y_{11}(s) \\ \vdots \\ \left(\sum_{n=1}^{N} \frac{\tilde{k}_n}{s - \bar{p}_n} \right) Y_{MM}(s) \end{bmatrix}$$

$$= \begin{bmatrix} Y_{11}(s) \\ \vdots \\ Y_{MM}(s) \end{bmatrix}. \quad (11)$$

Note that in (11), the poles of the scaling function $\sigma(s)$ are considered to be same as the poles of the approximated scaled functions $(\sigma Y_{11})(s), (\sigma Y_{22})(s), \dots (\sigma Y_{MM})(s)$. Also note here that, $\bar{p}_n$ represents the initial guess of poles and the total number of unknowns are $N_t = 2M + (M+1)N$. The ambiguity in the solution of the scaling function in (7) has been overcome by forcing it to approach unity at very high frequencies. Writing each row of (11) at k different frequency points $(k > 2N + 2)$, we get an overdetermined problem

$$\boldsymbol{A}X = \boldsymbol{b} \quad (12)$$

where (13)–(15) are shown at the bottom of the next page. The overdetermined problem of (12) is solved by least-square technique or QR factorization. In the case of least-square method, premultiplying both sides of (12) by $\boldsymbol{A}^t$, we get

$$\boldsymbol{A}^t \boldsymbol{A}\boldsymbol{X} = \boldsymbol{A}^t \boldsymbol{b}; \Rightarrow \boldsymbol{X} = (\mathbf{A}^t \boldsymbol{A})^{-1} \boldsymbol{A}^t \boldsymbol{b}. \quad (16)$$

On the other hand, in the case of using QR factorization, writing $\boldsymbol{A}$ in terms of QR factors, we get $\boldsymbol{A} = \boldsymbol{Q}\boldsymbol{R}$. Here $\boldsymbol{Q}$ is an orthogonal matrix, i.e., $\boldsymbol{Q}^t \boldsymbol{Q} = \boldsymbol{I}$, and $\boldsymbol{R}$ is an upper triangular matrix. Using this information and multiplying both sides of (12) by $\boldsymbol{Q}^t$, we get

$$\boldsymbol{R}\boldsymbol{X} = \boldsymbol{Q}^t \boldsymbol{b}; \Rightarrow \boldsymbol{X} = \mathbf{R}^{-1} \boldsymbol{Q}^t \boldsymbol{b}. \quad (17)$$

Next, a rational-function approximation for the function $\boldsymbol{Y}_{\text{diag}}(s)$ can be easily obtained by writing it in the fractional

form. For this purpose, we first express the scaling (7) and scaled (8) functions in fractional form as

$$\sigma(s) = \frac{\prod_{n=1}^{N}(s-\tilde{z}_n)}{\prod_{n=1}^{N}(s-\bar{p}_n)} \tag{18}$$

and

$$(\sigma \boldsymbol{Y}_{\text{diag}})(s) = \frac{1}{\prod_{n=1}^{N}(s-\bar{p}_n)} \begin{bmatrix} \hat{h}^{11}\prod_{n=1}^{N+1}\left(s-\hat{z}_n^{11}\right) \\ \hat{h}^{22}\prod_{n=1}^{N+1}\left(s-\hat{z}_n^{22}\right) \\ \vdots \\ \hat{h}^{MM}\prod_{n=1}^{N+1}\left(s-\hat{z}_n^{MM}\right) \end{bmatrix}. \tag{19}$$

From (9) it is evident that

$$\boldsymbol{Y}_{\text{diag}}(s) = \frac{(\sigma \boldsymbol{Y}_{\text{diag}})(s)}{\sigma(s)}. \tag{20}$$

Substituting (18) and (19) in (20), $\boldsymbol{Y}_{\text{diag}}(s)$ becomes

$$\begin{aligned} \boldsymbol{Y}_{\text{diag}}(s) &= \frac{(\sigma \boldsymbol{Y}_{\text{diag}})(s)}{\sigma(s)} \\ &= \frac{1}{\prod_{n=1}^{N}(s-\tilde{z}_n)} \begin{bmatrix} \hat{h}^{11}\prod_{n=1}^{N+1}\left(s-\hat{z}_n^{11}\right) \\ \vdots \\ \hat{h}^{MM}\prod_{n=1}^{N+1}\left(s-\hat{z}_n^{MM}\right) \end{bmatrix}. \end{aligned} \tag{21}$$

From (21) and (18), it is clear that the zeros of $\sigma(s)$ are the poles of $\boldsymbol{Y}\text{diag}(s)$. (*Note that the initial poles cancel in the division process as we started with the same initial poles for* $\sigma(s)$ *and* $(\sigma \boldsymbol{Y}_{\text{diag}})(s)$). Thus, by calculating the zeros of $\sigma(s)$ we get a better set of poles than the initial set of poles $\bar{p}_n$, for fitting the original function $\boldsymbol{Y}_{\text{diag}}(s)$. Once the vector of unknowns, $\boldsymbol{X}$ [(13)] is computed [using (16) or (17)], zeros of $\sigma(s)$ can be calculated, depending on whether the initial guess for the poles is real or complex, as follows.

Case 1: Real Poles: It is to be noted that zeros of $\sigma(s)$ correspond to the eigenvalues of the matrix [12]

$$\boldsymbol{H} = \boldsymbol{\Psi} - \boldsymbol{g}\phi^t \tag{22}$$

where

$$\Psi = \begin{bmatrix} \bar{p} & & & \\ & \bar{p} & & \\ & & \ddots & \\ & & & \bar{p}_N \end{bmatrix}$$

$$\boldsymbol{g} = \begin{bmatrix} 1 \\ 1 \\ \vdots \\ 1 \end{bmatrix}_{N\times 1}$$

$$\phi^t = [\tilde{k}_1 \tilde{k}_2 \ldots \tilde{k}_N]_{1\times N}. \tag{23}$$

Notice that Ψ is the diagonal matrix of starting (initial guess) poles, $\boldsymbol{g}$ is a unity column vector. ϕ is the column vector of residues of $\sigma(s)$, corresponding to the starting poles [computed using (16) or (17)].

Case 2: Complex Poles: In this case, too, zeros of $\sigma(s)$ correspond to the eigenvalues of the matrix $\boldsymbol{H}$ of (22), however, with $\boldsymbol{\Psi}$, $\boldsymbol{g}$ and ϕ modified as [12], you have (24) shown at the bottom of the next page. Once the zeros of $\sigma(s)$ are calculated, they are used as the new set of starting poles in the next iteration while solving (11). The next iteration provides new set of zeros of $\sigma(s)$ which are again used in the next iteration as starting poles. The iterative process is continued till the poles converge. It is to be noted that during this iterative process, some of the calculated poles may become unstable, i.e., the real part of some of the poles may be positive. This problem is overcome by inverting the sign of their real parts [12].

$$\boldsymbol{X} = [\hat{k}_1^{11} \ \ldots \ \hat{k}_N^{11} \ \hat{c}^{11} \ \hat{h}^{11} \ \hat{k}_1^{22} \ \ldots \ \hat{k}_N^{22} \ \hat{c}^{22} \ \hat{h}^{22} \ \ldots \ \hat{k}_1^{MM} \ \ldots \ \hat{k}_N^{MM} \ \hat{c}^{MM} \ \hat{h}^{MM} \ \tilde{k}_1 \ \ldots \ \tilde{k}_N] \tag{13}$$

$$\boldsymbol{b} = [Y_{11}(s_1) \ \ldots \ Y_{11}(s_k) \ Y_{22}(s_1) \ \ldots \ Y_{22}(s_k) \ \ldots \ Y_{MM}(s_1) \ \ldots \ Y_{MM}(s_k)]^t \tag{14}$$

$$\boldsymbol{A} = \begin{bmatrix} \frac{1}{s_1-\bar{p}_1} & \ldots & \frac{1}{s_1-\bar{p}_N} & 1 & s_1 & 0 & \ldots & 0 & 0 & 0 & \ldots & \ldots & \ldots & \ldots & \ldots & \ldots & \frac{-Y_{11}(s_1)}{s_1-\bar{p}_1} & \ldots & \frac{-Y_{11}(s_1)}{s_1-\bar{p}_N} \\ \vdots & & \vdots & & \vdots & \vdots & & & \vdots & & \ldots & \ldots & \ldots & \ldots & \ldots & \ldots & \vdots & & \vdots \\ \frac{1}{s_k-\bar{p}_1} & \ldots & \frac{1}{s_k-\bar{p}_N} & 1 & s_k & 0 & \ldots & 0 & 0 & 0 & \ldots & \ldots & \ldots & \ldots & \ldots & \ldots & \frac{-Y_{11}(s_k)}{s_k-\bar{p}_1} & \ldots & \frac{-Y_{11}(s_k)}{s_k-\bar{p}_N} \\ 0 & \ldots & 0 & 0 & 0 & \frac{1}{s_1-\bar{p}_1} & \ldots & \frac{1}{s_1-\bar{p}_N} & 1 & s_1 & \ldots & \ldots & \ldots & \ldots & \ldots & \ldots & \frac{-Y_{22}(s_1)}{s_1-\bar{p}_1} & \ldots & \frac{-Y_{22}(s_1)}{s_1-\bar{p}_N} \\ \vdots & & \vdots & & & \vdots & & \vdots & & \vdots & \ldots & \ldots & \ldots & \ldots & \ldots & \ldots & \vdots & & \vdots \\ 0 & \ldots & 0 & 0 & 0 & \frac{1}{s_k-\bar{p}_1} & \ldots & \frac{1}{s_k-\bar{p}_N} & 1 & s_k & \ldots & \ldots & \ldots & \ldots & \ldots & \ldots & \frac{-Y_{22}(s_k)}{s_k-\bar{p}_1} & \ldots & \frac{-Y_{22}(s_k)}{s_k-\bar{p}_N} \\ \vdots & & \vdots & & & \vdots & & \vdots & & \vdots & & \vdots & & \vdots & & & \vdots & & \vdots \\ 0 & \ldots & 0 & 0 & 0 & 0 & \ldots & 0 & 0 & 0 & \ldots & \frac{1}{s_1-\bar{p}_1} & \ldots & \frac{1}{s_1-\bar{p}_N} & 1 & s_1 & \frac{-Y_{MM}(s_1)}{s_1-\bar{p}_1} & \ldots & \frac{-Y_{MM}(s_1)}{s_1-\bar{p}_N} \\ \vdots & & \vdots & & & \vdots & & \vdots & & \vdots & & \vdots & & \vdots & & & \vdots & & \vdots \\ 0 & \ldots & 0 & 0 & 0 & 0 & \ldots & 0 & 0 & 0 & \ldots & \frac{1}{s_k-\bar{p}_1} & \ldots & \frac{1}{s_k-\bar{p}_N} & 1 & s_k & \frac{-Y_{MM}(s_k)}{s_k-\bar{p}_1} & \ldots & \frac{-Y_{MM}(s_k)}{s_k-\bar{p}_N} \end{bmatrix} \tag{15}$$

The above approach overcomes the illconditioning problem discussed in Section II and also ensures that the poles of the admittance matrix are common. This avoids the conventional method of independently fitting individual admittance parameters and then collecting the common set of poles. Also, it helps to keep the macromodel compact and enables efficient transient simulation.

IV. Residue Computation and Proposed Linear Passivity Constraints (Step 2)

Once an accurate set of poles are calculated in Step-1, each element of $\boldsymbol{Y}(s)$ can be expressed in the pole-residue formulation as

$$Y_{ij}(s) = c^{i,j} + \frac{k_1^{i,j}}{s-p_1} + \frac{k_2^{i,j}}{s-p_2} + \cdots + \frac{k_N^{i,j}}{s-p_N}, \quad (i,j = 1,2,\ldots M) \tag{25}$$

where, $p_i, p_2 \ldots p_N$ are the poles of the system, $k_i, k_2 \ldots k_N$ are the corresponding residues and c is the direct coupling constant. The residues of each element of $\boldsymbol{Y}(s)$ of can be computed by formulating a linear least-square problem by writing (25) at several frequency points. However, direct application of this approach does not guarantee the passivity of the resulting macromodel. For a macromodel with stable poles, to ensure passivity, (3) must be satisfied. However, ensuring (3) is a difficult task and its direct application can lead to nonlinear optimization problem. In order to address these difficulties, we propose the following algorithm with linear constraints, which help to retain the passivity of the macromodel.

Let the tabulated data be given up to a maximum frequency $\omega_{\max}$. Note that, in practice $\omega_{\max}$ is determined based on the rise time of the input signal (t_r) using the relationship: $\omega_{\max} = (2\pi \times 0.35)/t_r$ [1]. The common pole-set $\boldsymbol{P}$ obtained from Step 1, written in ascending order of their imaginary parts, can be expressed as

$$\begin{aligned} \boldsymbol{P} &= [p_1, p_2 \ldots p_{\max 0}, p_{\max 1} \ldots, p_N]; \\ \operatorname{imag}(p_1) &< \cdots < \cdots < \operatorname{imag}(p_N); \\ \operatorname{imag}(p_{\max 0}) &< \omega_{\max} < \operatorname{imag}(p_{\max 1}). \end{aligned} \tag{26}$$

Consequently, the admittance matrix of (4) has the following form in (27) shown at the bottom of the page. The unknown residues $k_n^{i,j}$ and the direct coupling constants $c^{i,j}$ are computed by writing each entry of (27) at several frequency points, $\omega_1, \omega_2, \ldots \omega_{N_m}$, as

$$c^{i,j} + \frac{k_1^{i,j}}{s_m - p_1} + \frac{k_2^{i,j}}{s_m - p_2} + \cdots + \frac{k_N^{i,j}}{s_m - p_N} = Y_{ij}(s_m) \tag{28}$$

where s_m represents the mth frequency point. In the case of complex poles, both the pole as well as its conjugate should be used while formulating (28). Next, equating both the real and imaginary parts of (28) separately, we obtain a new set of linear equations as

$$\boldsymbol{A}\boldsymbol{X}^{i,j} = \boldsymbol{b}^{i,j} \Rightarrow \begin{bmatrix} Re(\boldsymbol{A}) \\ Im(\boldsymbol{A}) \end{bmatrix} \mathbf{X}^{i,j} = \begin{bmatrix} Re(\boldsymbol{b}^{i,j}) \\ Im(\boldsymbol{b}^{i,j}) \end{bmatrix} \tag{29}$$

where $\boldsymbol{X}^{i,j} \in \Re^{(N+1)\times 1}$ is the column vector containing the unknowns corresponding to the real and imaginary parts of residues, $\boldsymbol{b}^{i,j} \in C^{N_m \times 1}$ is the column vector containing real and imaginary parts of frequency responses (represented by admittance parameters $Y_{i,j}(s_m)$) and $\boldsymbol{A} \in C^{N_m \times (N+1)}$ consists of entries contributed by the LHS of (28).

When written at several frequency points, (29) can be formulated as a least square problem [similar to formulation in (16)], which is solved subjected to a new set of proposed passivity conforming linear constraints [22], as

$$\begin{bmatrix} Re(\boldsymbol{A}) \\ Im(\boldsymbol{A}) \end{bmatrix}^t \begin{bmatrix} Re(\boldsymbol{A}) \\ Im(\boldsymbol{A}) \end{bmatrix} \boldsymbol{X}^{i,j} = \begin{bmatrix} Re(\boldsymbol{A}) \\ Im(\boldsymbol{A}) \end{bmatrix}^t \begin{bmatrix} Re(\boldsymbol{b}^{i,j}) \\ Im(\boldsymbol{b}^{i,j}) \end{bmatrix} \tag{30}$$

$$\begin{aligned} \boldsymbol{\Psi} &= \begin{bmatrix} \Psi_1 & & & \\ & \Psi_2 & & \\ & & \ddots & \\ & & & \Psi_N \end{bmatrix} \\ \boldsymbol{\Psi} &= \begin{bmatrix} Re(\bar{p}_i) & Im(\bar{p}_i) \\ -Im(\bar{p}_i) & Re(\bar{p}_i) \end{bmatrix}; \quad i = 1,2,\ldots N \\ \boldsymbol{g} &= [2 \quad 0 \quad 2 \quad 0 \ldots \quad 2 \quad 0]^t_{1\times 2N} \\ \phi^t &= [Re(\tilde{k}_1) \quad Im(\tilde{k}_1) \quad Re(\tilde{k}_2) \quad Im(\tilde{k}_2) \ldots Re(\tilde{k}_N) \quad Im(\tilde{k}_N)]_{1\times 2N} \end{aligned} \tag{24}$$

$$\boldsymbol{Y}(s) = \begin{bmatrix} c^{1,1} + \sum_{n=1}^{N} \frac{k_n^{1,1}}{s-p_n} & c^{1,2} + \sum_{n=1}^{N} \frac{k_n^{1,2}}{s-p_n} & \cdots & c^{1,M} + \sum_{n=1}^{N} \frac{k_n^{1,M}}{s-p_n} \\ \vdots & \vdots & \vdots & \\ c^{M,1} + \sum_{n=1}^{N} \frac{k_n^{M,1}}{s-p_n} & c^{M,2} + \sum_{n=1}^{N} \frac{k_n^{M,2}}{s-p_n} & \cdots & c^{M,M} + \sum_{n=1}^{N} \frac{k_n^{M,M}}{s-p_n} \end{bmatrix} \tag{27}$$

such that

a) ***for diagonal elements***, *i.e.*, $Y_{ij}(s)$, $i = j$

- the direct coupling constant

$$c^{i,j} \geq 0 \tag{C1}$$

- the real part of the computed function is equal to or greater than the real part of the given tabulated data, i.e.,

$$Re(\boldsymbol{AX}^{i,i}) \geq Re(\boldsymbol{b}^{i,i}) \geq 0 \tag{C2}$$

b) ***for off-diagonal elements***, *i.e.*, $Y_{ij}(s)$, $i \neq j$

- the direct coupling constant

$$c^{i,j} = 0 \tag{C3}$$

- any pole beyond the maximum frequency of interest $\omega_{\max}$ is ignored, i.e., the following poles are only considered from the common pole set in (26)

$$\boldsymbol{P} = [p_1, p_2 \ldots p_{\max 0}]. \tag{C4}$$

The above linear constraints (C1)–(C4) help in preserving passivity of the macromodel, by satisfying the passivity condition (3) (i.e, $Real(\boldsymbol{Y}(j\omega)) = [\boldsymbol{Y}^t(j\omega^*) + \boldsymbol{Y}(j\omega)]/2 \geq 0$) in the region $0 \leq \omega \leq \infty$. In the remainder of this section, a discussion of how this objective is achieved using the above constraints, is given.

a) Region $\omega = \infty$

It is obvious from the constraints (C1) and (C3), that the condition (3) is satisfied at $\omega = \infty$.

b) Region $0 \leq \omega \leq \omega_{\max}$

Constraint (C2) helps to ensure that the passivity condition (3) is satisfied in this region. This constraint is developed based on the following theorem [34].

Theorem -1 (Gershgorin's Theorem): Let $\boldsymbol{A} = [a_{ij}]$ be a square matrix. All the eigenvalues of $\boldsymbol{A}$ lie in the union of the discs centered at its diagonal entries a_{ii}, with radii equal to the sum of the absolute values of the off-diagonal entries in the respective row. i.e., if λ is an eigenvalue of $\boldsymbol{A}$, then for any i we have

$$|a_{ii} - \lambda| \leq \sum_{j \neq i} |a_{ij}|. \tag{31}$$

An example depicting the above theorem is given in Appendix A. Implications of this theorem and constraint (C2) can be explained as follows. Enforcing constraint (C2) helps to maintain the diagonal dominance of the computed model either same or more than that of the given data. This helps to avoid the violation of the passivity condition (3) in the regions where the data is marginally passive. It is to be noted that, in such regions, some of the eigenvalues of $Real(\boldsymbol{Y}(j\omega))$ will be very close to zero. Such eigenvalues are very sensitive to any error during the fitting of the given data. For the purpose of illustration, consider the original data in the marginally passive region, and a corresponding particular eigenvalue λ, which is close to zero. Let $\hat{\lambda}$ be the corresponding eigenvalue from the fitted data, such that

$$\hat{\lambda} = \lambda + \Delta\lambda. \tag{32}$$

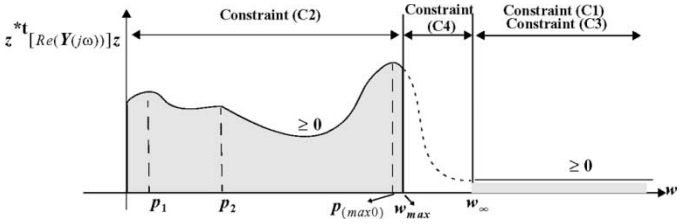

Fig. 2. Illustration of the general behavior of $Z^{*t}[Re(Y(j\omega))]z$ when using the proposed constraints.

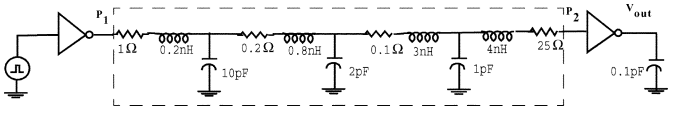

Fig. 3. Nonlinear circuit containing RLC lumped network.

Although the data is fairly accurately fit, however, due to the sensitive nature of such eigenvalues, any minor error can shift the eigenvalues in the fitted data to the negative region (i.e., resulting in passivity violation). Use of constraint (C2) ensures that the computed values of the real part of the diagonal entries is equal or greater than that of the given data. In other words, by the above theorem, the centre of the eigenvalue discs is shifted toward more positive region, and hence maintaining $\Delta\lambda$ of (32) to be always positive (i.e., the eigenvalues from the fitted data to be always positive). For data with many and wider marginally passive regions, an additional constraint for nondiagonal elements: $|Re(\boldsymbol{AX}^{i,j})| \leq |Re(\boldsymbol{b}^{i,j})|$, can be used in conjunction with (C2). Importance of the constraint (C2) is numerically illustrated in Example 2 of Section VI (Figs. 10 and 11).

c) Region $\omega_{\max} \leq \omega \leq \infty$:

Constraint (C4), in conjunction with constraints (C1) and (C3), helps to satisfy the passivity condition (3) in this region. This is because, since any pole beyond $\omega_{\max}$ is neglected for nondiagonal elements, and also since $c^{i,j} = 0$ for nondiagonal elements, the response of nondiagonal elements beyond $\omega_{\max}$ quickly tends to zero. In other words, these constraints avoid any large variations (which could happen if poles beyond $\omega_{\max}$ are considered for the nondiagonal elements) in nondiagonal element responses, there by minimizing the possibility of violation of the passivity condition (3) in this region.

A graphical description of the impact of these constraints while satisfying passivity condition (3), at various frequency regions is given in Fig. 2.

V. Passivity Check and Compensation (Step 3)

It is to be noted that, since the constraints defined in Section IV are not strict passivity enforcing conditions, there may be minor chances of passivity violation (as no constraints were imposed on the behavior of diagonal elements immediately after $\omega_{\max}$). Hence, the resulting macromodel is checked for any passivity violation. Traditional approach for this purpose is based on *frequency-sweep of eigenvalues of the real-part of the admittance matrix* $(Re(\boldsymbol{Y}(s)))$ of the macromodel. However, this approach suffers from several drawbacks, such as up to what frequency to sweep and how fine the sweep should be. In order

TABLE I
POLES AND RESIDUES OBTAINED USING THE PROPOSED METHOD (EXAMPLE 1)

Poles	R^{11}	R^{12} & R^{21}	R^{22}
-3.3385	1.2184e-001	-1.2723e-001	1.3286e-001
-6.2928	-7.3081e-009	-2.9387e-010	8.1838e-010
-1.9886e+000+1.7803e+001i	1.2620e+000-5.3718e-002i	1.9255e-001+3.8040e-002i	2.7689e-002+1.2787e-002i
-1.6406e+000 +2.4315e+001i	2.2657e-001+9.3384e-001i	-1.5918e-001+-4.1527e-002i	2.7124e-002+7.5762e-003i
-3.6021e-004 +2.4998e+001i	2.8816e-008+4.0828e-008i	-1.2337e-008+5.4798e-009i	4.5470e-010+1.3065e-009i
-4.0573e-001 +3.2744e+001i	2.4330e-001+1.1006e-001i	3.0242e-002+1.2548e-002i	3.7552e-003+1.4209e-003i

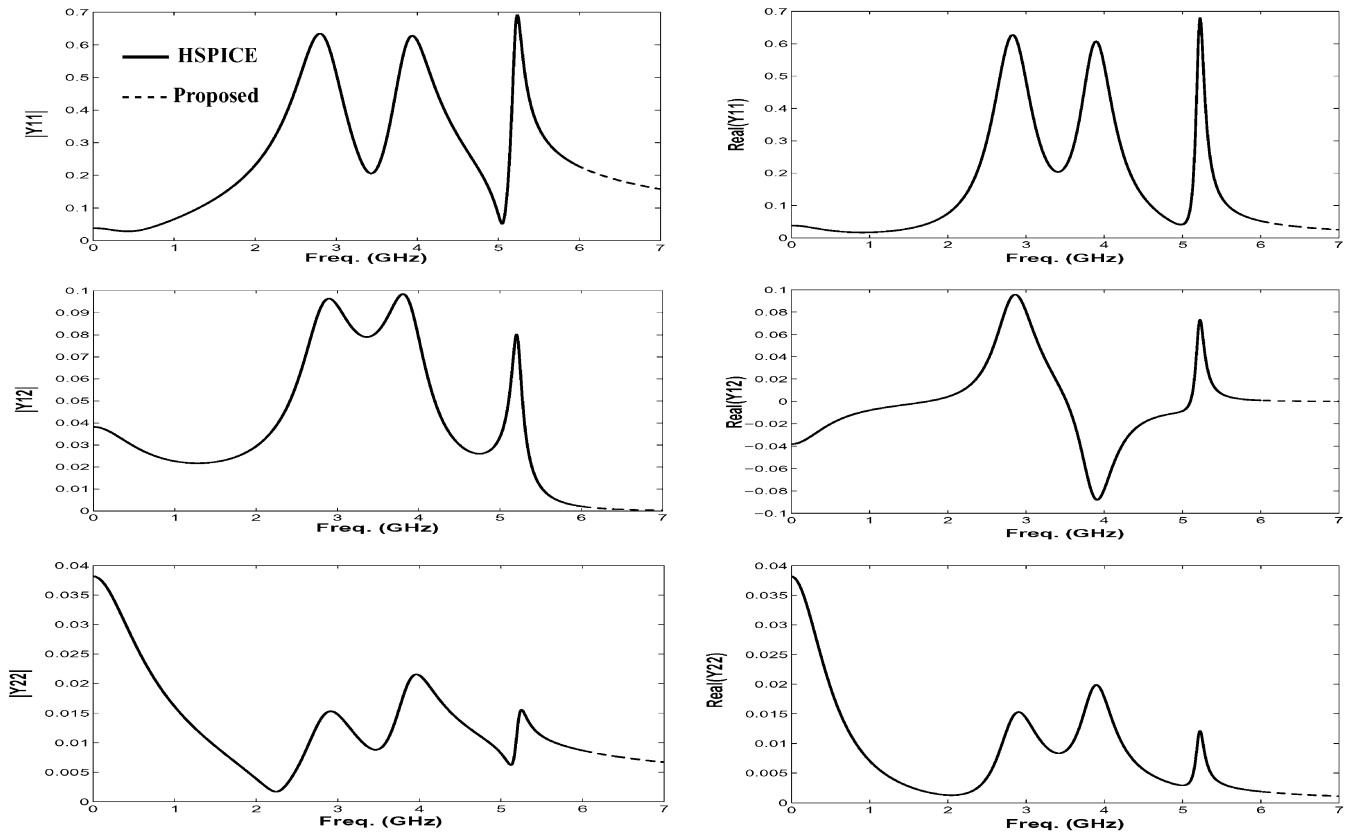

Fig. 4. Frequency responses for Example 1.

to avoid this problem, the following approach is developed in this paper.

Consider the state-space representation corresponding to the pole-residue macromodel of (27)

$$\begin{aligned} \dot{\boldsymbol{x}}(t) &= \boldsymbol{A}x(t) + \boldsymbol{B}u(t) \\ y(t) &= \boldsymbol{C}x(t) + \boldsymbol{D}u(t). \end{aligned} \tag{33}$$

Here, $\boldsymbol{A} \in \Re^{n\times n}$, $\boldsymbol{B} \in \Re^{n\times M}$, $\boldsymbol{C} \in \Re^{M\times n}$, $\boldsymbol{D} \in \Re^{M\times M}$, $\boldsymbol{u}(t) \in \Re^{M}$, $\boldsymbol{y}(t) \in \Re^{M}$, $\boldsymbol{x}(t) \in \Re^{n}$ (n is the total number of state variables) [24], [35], [36]. It is to be noted that the poles of the system are contained in matrix $\boldsymbol{A}$, residues in matrix $\boldsymbol{C}$, while the direct coupling constants are in matrix $\boldsymbol{D}$. Next, the following two theorems are used for systematic passivity verification without resorting to frequency sweep.

Theorem 2: The state-space system ($\boldsymbol{A}$, $\boldsymbol{B}$, $\boldsymbol{C}$, $\boldsymbol{D}$) is passive iff the following Hamiltonian matrix ($\boldsymbol{M}$) [37] has no imaginary eigenvalues:

$$\boldsymbol{M} = \begin{bmatrix} \boldsymbol{A} - \boldsymbol{B}(\boldsymbol{D} + \mathrm{D}^t)^{-1}\boldsymbol{C} & \boldsymbol{B}(\boldsymbol{D} + \boldsymbol{D}^t)^{-1}\boldsymbol{B}^t \\ -\boldsymbol{C}^t(\boldsymbol{D} + \boldsymbol{D}^t)^{-1}\boldsymbol{C} & -\boldsymbol{A}^t + \boldsymbol{C}^t(\boldsymbol{D} + \boldsymbol{D}^t)^{-1}\mathrm{B}^t \end{bmatrix}. \tag{34}$$

In case of passivity violation, the following theorem helps in identifying the exact location of passivity violation.

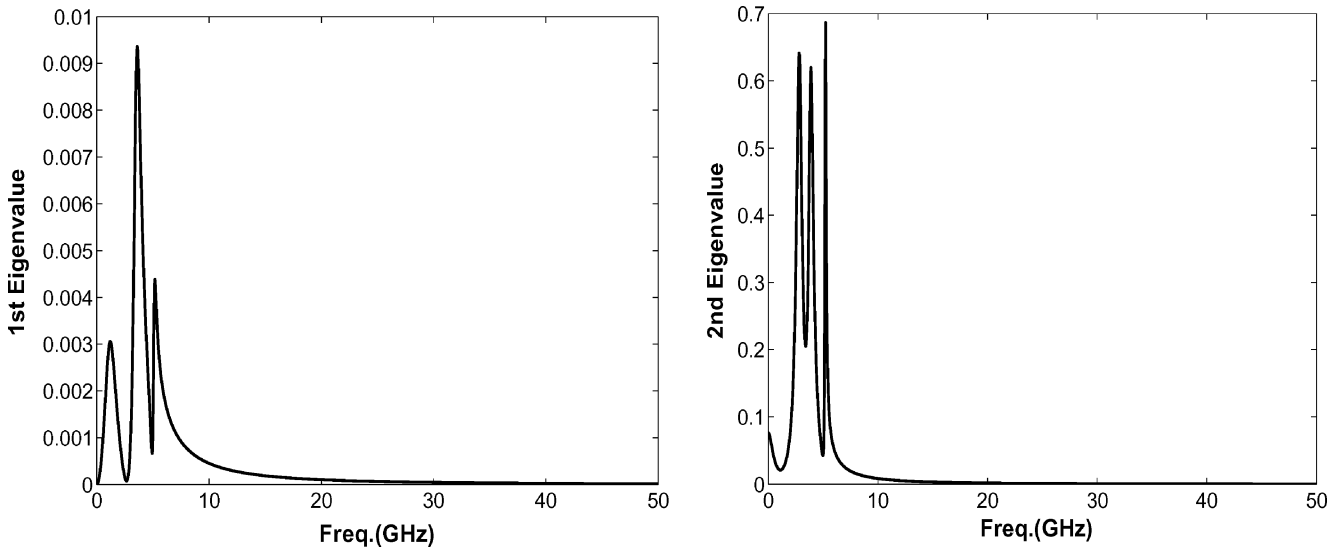

Fig. 5. Eigenvalues of $Real(Y(s))$ for Example 1.

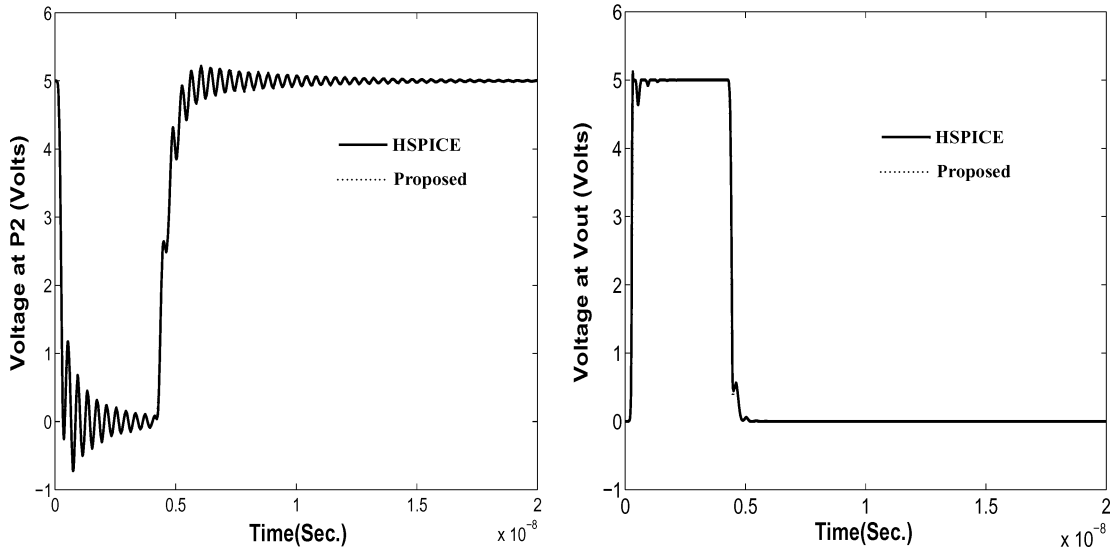

Fig. 6. Time-domain responses for Example 1.

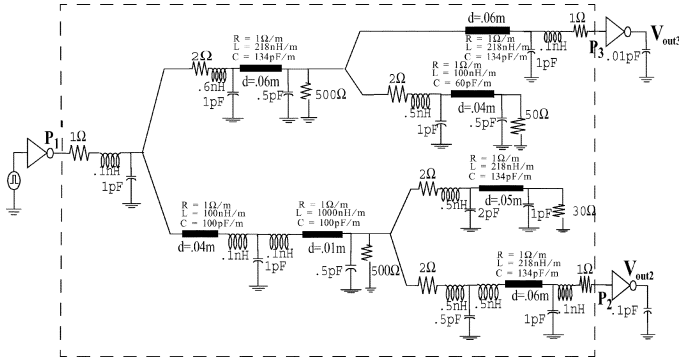

Fig. 7. Three-port interconnect subnetwork (Example 2).

Theorem 3: The real part of the symmetric admittance matrix, $\boldsymbol{F}(j\omega_0)$, is singular if $j\omega_a$ is an eigenvalue of the corresponding Hamiltonian matrix $\boldsymbol{M}$, provided $\boldsymbol{D}+\boldsymbol{D}^t$ is a positive definite matrix [30], [38].

Note that, in case a macromodel is found to be nonpassive, Theorem 3 gives a very useful information about the exact locations where the violation is happening. This information can be used to carry out the passivity compensation by the approaches such as [29], [31], [32]. The proof of Theorem-3 can be found in [38]. An alternative and simpler proof is given in Appendix B. Note that, for the case of state-space matrices ($\boldsymbol{A}, \boldsymbol{B}, \boldsymbol{C}, \boldsymbol{D}$) corresponding to scattering parameters, the criteria for passivity is that the norm of scattering matrix be less than or equal to one for $\omega \in \Re \cup \infty$ [21]. Also for this case, a similar result as Theorem 3 can be obtained: "the Hamiltonian matrix of the nonpassive macromodel has imaginary eigenvalues which correspond to the exact locations where the norm of the corresponding scattering matrix becomes equal to one." Having ensured the passivity of the matrix-transfer function, a time-domain macromodel can be synthesized as a set of first-order differential equations [1], which can be easily linked to nonlinear simulators since they are described in the time domain. Alternatively, they can be directly

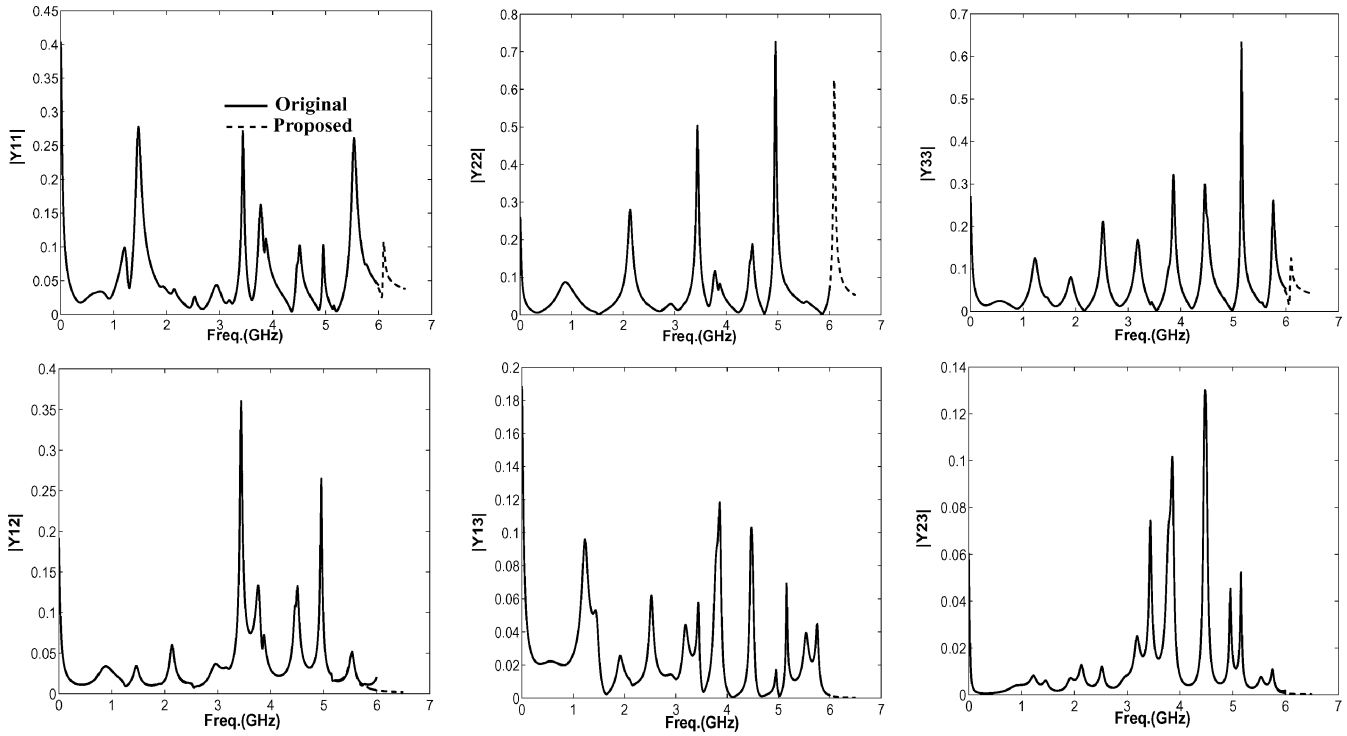

Fig. 8. Frequency responses (magnitude) for Example 2.

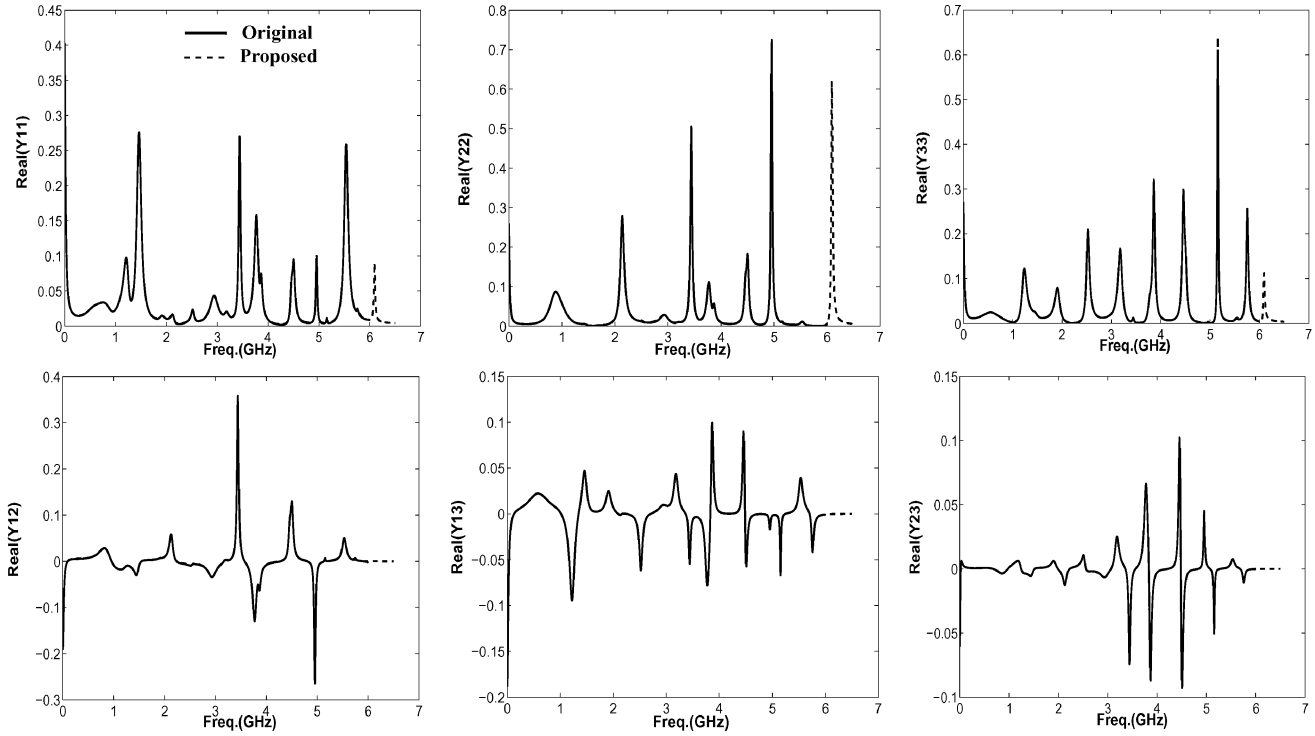

Fig. 9. Frequency responses (real part) for Example 2.

stamped to the simulator, based on simulator interface capabilities such as Laplace element of HSPICE [39].

VI. Computational Results

In this section, two examples are presented to demonstrate the efficiency and accuracy of the proposed algorithm.

Example 1- Two Port R,L,C Circuit: In this example, a relatively small RLC network (Fig. 3) is analyzed using the proposed technique. The linear part of the network is simulated using HSPICE to obtain admittance parameters at 1000 frequency points up to 6 GHz, and is considered as tabulated data (input) to the proposed algorithm. Using the proposed method, a common pole set (with two real poles and four

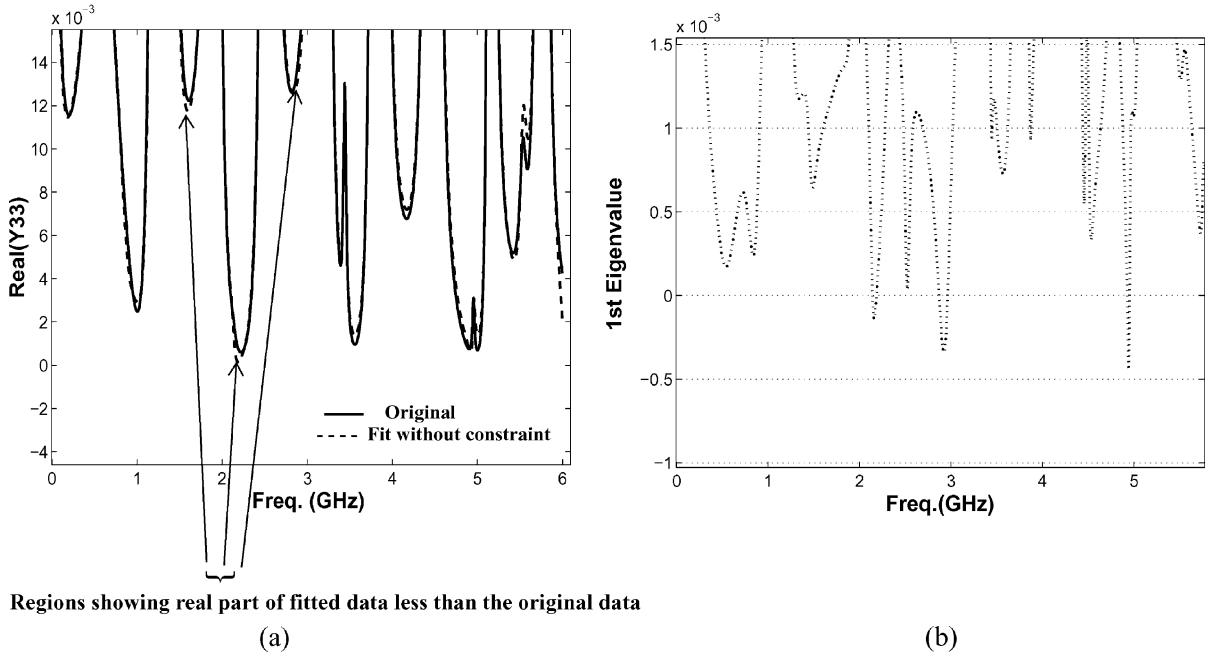

Fig. 10. Illustration of passivity violation due to unconstrained fitting (without using constraint (C2)).

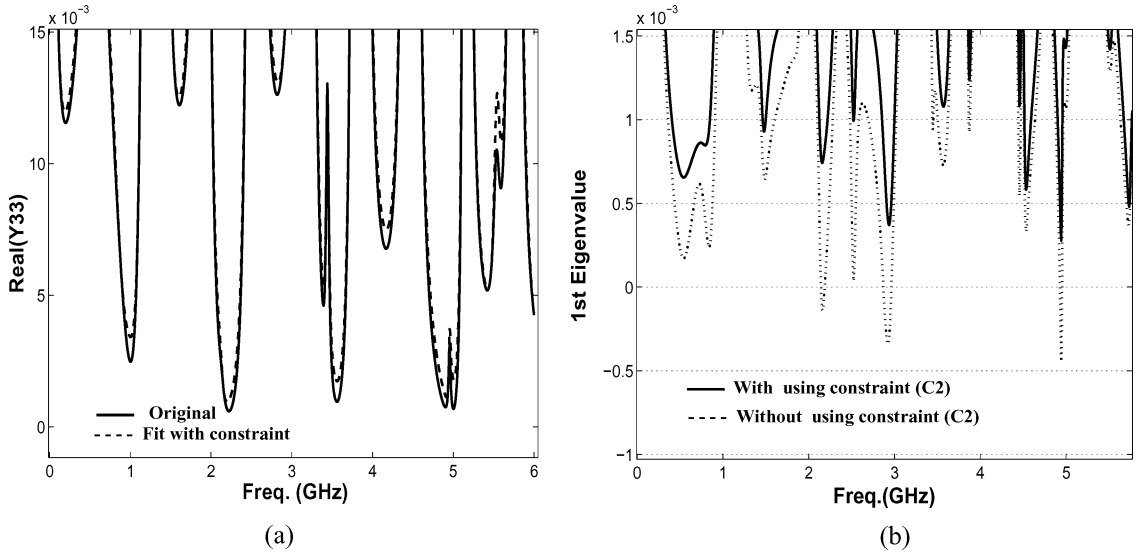

Fig. 11. Illustration of the fitting and eigenvalue spectrum when constraint (C2) is used.

complex poles) and subsequently residues are computed (given in Table I; values are scaled by 1e9). The computed direct coupling constants, for diagonal elements $Y_{11}(s)$, $Y_{22}(s)$ are 1.9291e–06 and 6.8651e–08, respectively (zero for off-diagonal elements). Fig. 4 shows the comparison of frequency responses obtained using the proposed method and HSPICE, and they match accurately. Next, the state-space macromodel is checked for passivity using Theorem -2, by finding the eigenvalues of the Hamiltonian matrix in (34) and no imaginary eigenvalues were found (i.e., the macromodel is passive). This is also demonstrated using the conventional approach, by plotting the eigenvalues of the $Re(\boldsymbol{Y}(j\omega))$ against frequency up to 50 GHz (Fig. 5). Since the eigenvalues are positive even up to 50 GHz, implies that the macromodel is passive. Next, the macromodel obtained from the proposed method is linked to HSPICE and a nonlinear analysis is performed. The network is excited with a trapezoidal pulse having a rise/fall time of 0.1 ns and a pulse width of 4 ns. Responses at nodes $\mathbf{P}_2$ and $\mathbf{V}_{\rm out}$ are compared with the HSPICE simulation of the original network in Fig. 6. As seen, the results from both the methods match accurately.

Example 2: 3-Port Measured Data: In this example, the proposed algorithm was performed on a set of measured data (obtained from a known 3-port interconnect network, given in Fig. 7). The data is (Y-parameter) given up to 6 GHz, at 1000 sample points and is fitted using the proposed method (40 complex poles and 4 real poles were required). Figs. 8 and 9 show the comparison between the original data and the response of the proposed model and they match accurately. Figs. 10 and 11 illustrate the usefulness of constraint (C2). Fig. 10(a) shows (using enlarged vertical axis) the comparison

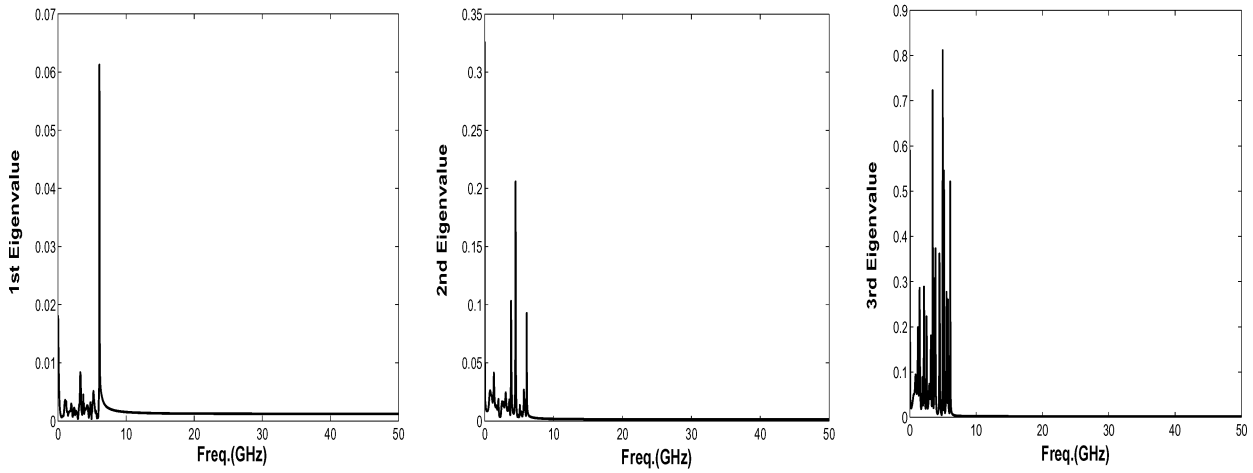

Fig. 12. Eigenvalue spectrum of $Real(Y(s))$ of the proposed macromodel (Example 2).

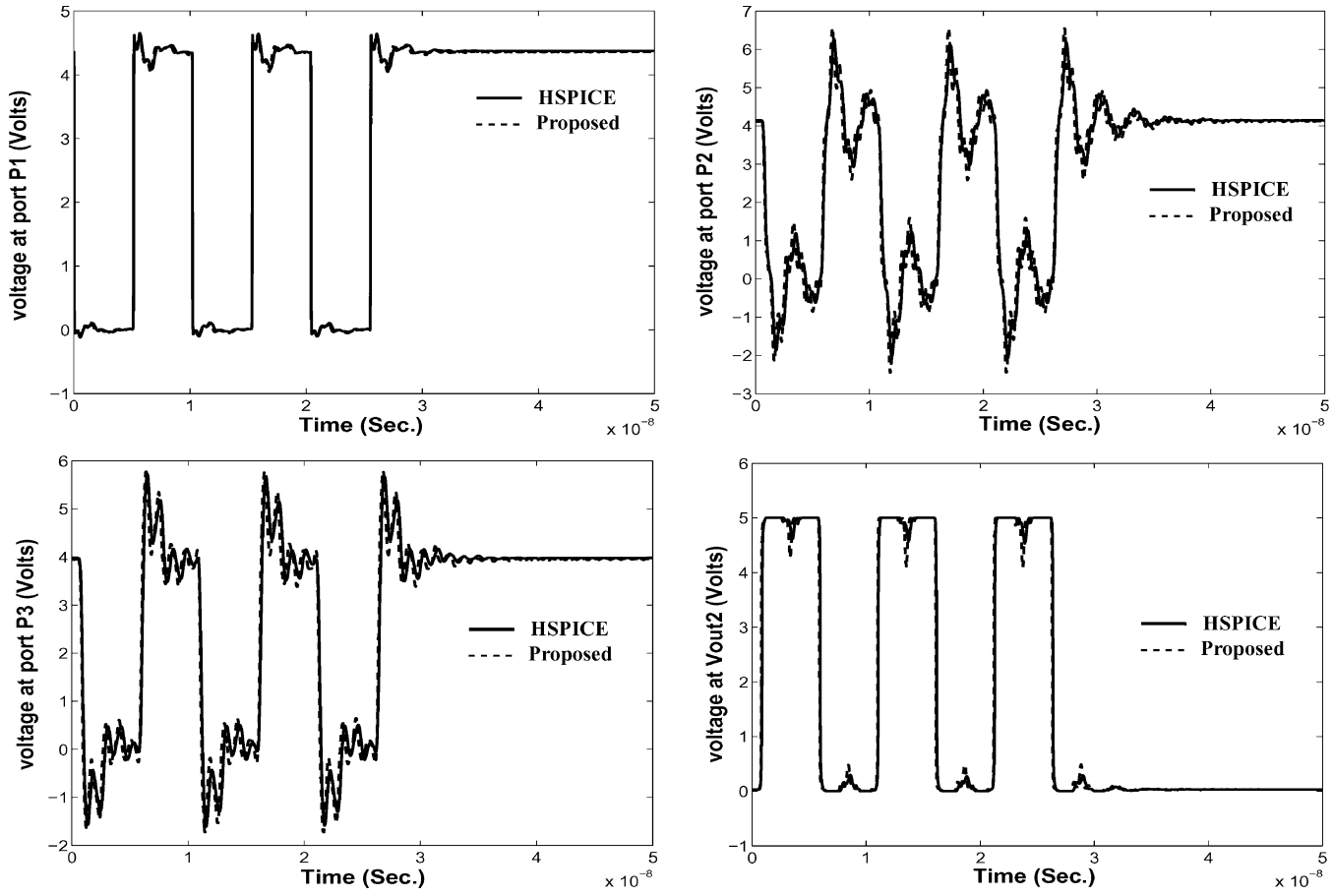

Fig. 13. Transient results for Example 2.

of original $real(Y_{33}(s))$ with the response of the computed model obtained without using constraint (C2). As seen, at certain frequencies, the fitted response is slightly smaller than the original data and the corresponding eigenvalue spectrum [Fig. 10(b)] contains several negative values. Fig. 11 shows the improved results when the constraint (C2) is enforced and the eigenvalue spectrum in this case always remained positive [Fig. 11(b)].

Next, the state-space macromodel is checked for passivity using Theorem -2, by finding the eigenvalues of the Hamiltonian matrix in (34) and no imaginary eigenvalues were found (i.e., the macromodel is passive). This is also demonstrated using the conventional approach, by plotting the eigenvalues of the $Re(\boldsymbol{Y}(j\omega))$ against frequency up to 50 GHz (Fig. 12). As seen, the eigenvalues are positive even up to 50 GHz, indicating that the macromodel is passive. Next the macromodel is linked to

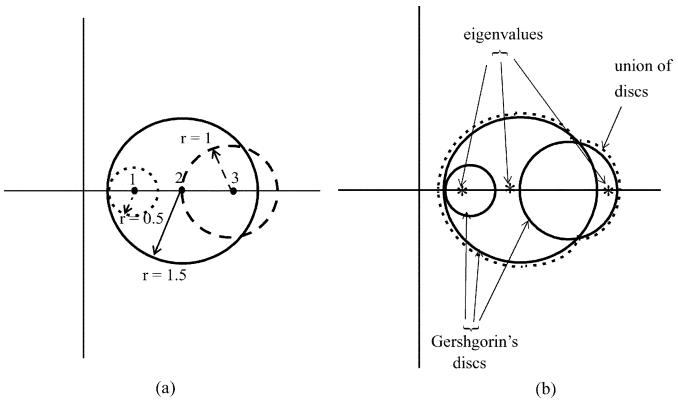

Fig. 14. Gershgorin's discs for the matrix of (35).

HSPICE and a nonlinear analysis is performed. The network is excited by a pulse having a rise and fall time of 0.1 ns. The results at node $\mathbf{P}_1$, $\mathbf{P}_2$, $\mathbf{P}_3$, $\boldsymbol{V}_{\text{out2}}$ are shown in Fig. 13, in comparison to the HSPICE simulation of the original circuit (from which the measured data was obtained) and they match accurately.

VII. Conclusion

In this paper, an efficient algorithm has been presented for transient simulation of linear subnetworks characterized by simulated/measured data in the presence of other linear and nonlinear devices. New linear constraints have been proposed, which help in preserving the passivity of resulting macromodels. Accurate and fast passivity verification strategy has been presented.

Appendix A

In this appendix, an illustrative example is provided, describing the Gershgorin's theorem (Theorem -1, stated in Section IV).

Consider the following matrix:

$$\begin{bmatrix} 2 & 1 & 0.5 \\ 1 & 3 & 0 \\ 0.5 & 0 & 1 \end{bmatrix}. \tag{35}$$

Corresponding Gershgorin's discs are depicted in Fig. 14.

Since the matrix in (35) is of size 3×3, it has three discs as shown in Fig. 14(a), with the centres at 2, 3, and 1, and the corresponding radii of 1.5, 1, and 0.5, respectively. As per Gershgorin's theorem, eigenvalues of the matrix in (35) lie in the union of these three discs, shown by the dotted curve in Fig. 14(b). As a verification, it can be noted that the eigenvalues (0.70, 1.64, 3.64) indicated by "*" in Fig. 14(b), lie inside the union of the corresponding Gershgorin's discs.

Appendix B
Proof of Theorem 3

Assume that $j\omega_0$ is an eigenvalue of the Hamiltonian matrix $\boldsymbol{M}$, i.e.,

$$\boldsymbol{M}\begin{bmatrix} \boldsymbol{r} \\ \boldsymbol{s} \end{bmatrix} = j\omega_0 \begin{bmatrix} \boldsymbol{r} \\ \boldsymbol{s} \end{bmatrix} \tag{36}$$

where, $[\boldsymbol{r} \quad \boldsymbol{s}]^t$ is the eigenvector of $\boldsymbol{M}$ corresponding to the eigenvalue $j\omega_0$. Using (34) and (36), we get

$$\begin{bmatrix} \boldsymbol{A}-\boldsymbol{B}(\boldsymbol{D}+\boldsymbol{D}^t)^{-1}\boldsymbol{C} & \boldsymbol{B}(\boldsymbol{D}+\boldsymbol{D}^t)^{-1}\boldsymbol{B}^t \\ -\boldsymbol{C}^t(\boldsymbol{D}+\boldsymbol{D}^t)^{-1}\boldsymbol{C} & -\boldsymbol{A}^t+\boldsymbol{C}^t(\boldsymbol{D}+\boldsymbol{D}^t)^{-1}\boldsymbol{B}^t \end{bmatrix}\begin{bmatrix} \boldsymbol{r} \\ \boldsymbol{s} \end{bmatrix} = j\omega_0 \begin{bmatrix} \boldsymbol{r} \\ \boldsymbol{s} \end{bmatrix}. \tag{37}$$

Notice in (37) that, $(\boldsymbol{D}+\boldsymbol{D}^t)^{-1}$ exists, as it is assumed that $(\boldsymbol{D}+\boldsymbol{D}^t)$ is positive definite. Rearranging (37), we have

$$\begin{bmatrix} -\boldsymbol{B}(\boldsymbol{D}+\boldsymbol{D}^t)^{-1}\boldsymbol{C} & \boldsymbol{B}(\boldsymbol{D}+\boldsymbol{D}^t)^{-1}\boldsymbol{B}^t \\ -\boldsymbol{C}^t(\boldsymbol{D}+\boldsymbol{D}^t)^{-1}\boldsymbol{C} & \boldsymbol{C}^t(\boldsymbol{D}+\boldsymbol{D}^t)^{-1}\boldsymbol{B}^t \end{bmatrix}\begin{bmatrix} \boldsymbol{r} \\ \boldsymbol{s} \end{bmatrix} = j\omega_0 \begin{bmatrix} \boldsymbol{r} \\ \boldsymbol{s} \end{bmatrix} + \begin{bmatrix} -\boldsymbol{A} & \\ & \boldsymbol{A}^t \end{bmatrix}\begin{bmatrix} \boldsymbol{r} \\ \boldsymbol{s} \end{bmatrix}. \tag{38}$$

After simple mathematical manipulations (38) can be written as

$$\begin{bmatrix} \boldsymbol{B} \\ \boldsymbol{C}^t \end{bmatrix}(\boldsymbol{D}+\boldsymbol{D}^t)^{-1}\begin{bmatrix} -\boldsymbol{C} & \boldsymbol{B}^t \end{bmatrix}\begin{bmatrix} \boldsymbol{r} \\ \boldsymbol{s} \end{bmatrix} = \begin{bmatrix} (j\omega_0\boldsymbol{I}-\boldsymbol{A}) & \\ & (j\omega_0\boldsymbol{I}+\boldsymbol{A}^t) \end{bmatrix}\begin{bmatrix} \boldsymbol{r} \\ \boldsymbol{s} \end{bmatrix} \tag{39}$$

which can rewritten as

$$\begin{bmatrix} \boldsymbol{B} \\ \boldsymbol{C}^t \end{bmatrix} u = \begin{bmatrix} (j\omega_0\boldsymbol{I}-\boldsymbol{A}) & \\ & (j\omega_0\boldsymbol{I}+\boldsymbol{A}^t) \end{bmatrix}\begin{bmatrix} \boldsymbol{r} \\ \boldsymbol{s} \end{bmatrix} \tag{40}$$

or

$$\begin{bmatrix} s \\ s \end{bmatrix}\begin{bmatrix} (j\omega_0\boldsymbol{I}-\boldsymbol{A}) & \\ & (j\omega_0\boldsymbol{I}+\boldsymbol{A}^t) \end{bmatrix}^{-1}\begin{bmatrix} \mathbf{B} \\ \boldsymbol{C}^t \end{bmatrix}\boldsymbol{u} \tag{41}$$

where

$$\boldsymbol{u} = (\boldsymbol{D}+\boldsymbol{D}^t)^{-1}\begin{bmatrix} -\boldsymbol{C} & \boldsymbol{B}^t \end{bmatrix}\begin{bmatrix} \boldsymbol{r} \\ \boldsymbol{s} \end{bmatrix}. \tag{42}$$

Using (41) and (42), we get

$$(\boldsymbol{D}+\boldsymbol{D}^t)\boldsymbol{u} = \begin{bmatrix} -\boldsymbol{C} & \boldsymbol{B}^t \end{bmatrix} \times \begin{bmatrix} (j\omega_0\boldsymbol{I}-\boldsymbol{A})^{-1} & \\ & (j\omega_0\boldsymbol{I}+\boldsymbol{A}^t)^{-1} \end{bmatrix}\begin{bmatrix} \boldsymbol{B} \\ \boldsymbol{C}^t \end{bmatrix}\boldsymbol{u}. \tag{43}$$

Equation (43) can be rearranged as

$$(\boldsymbol{D}+\boldsymbol{D}^t)\boldsymbol{u} = \begin{bmatrix} -\boldsymbol{C} & \boldsymbol{B}^t \end{bmatrix}\begin{bmatrix} (j\omega_0\boldsymbol{I}-\boldsymbol{A})^{-1}\boldsymbol{B} \\ (j\omega_0\boldsymbol{I}+\boldsymbol{A}^t)^{-1}\boldsymbol{C}^t \end{bmatrix}\boldsymbol{u} \tag{44}$$

or

$$(\boldsymbol{C}(j\omega_0\boldsymbol{I}-\boldsymbol{A})^{-1}\boldsymbol{B}+\boldsymbol{D}+\boldsymbol{B}^t(-j\omega_0\boldsymbol{I}-\boldsymbol{A}^t)^{-1}\boldsymbol{C}^t+\mathbf{D}^t)\boldsymbol{u} = 0. \tag{45}$$

Using (3), we can write (45) as

$$\boldsymbol{F}(j\omega_0)\boldsymbol{u} = 0. \tag{46}$$

It is evident from (45) that $\boldsymbol{F}(j\omega)$ is singular at $j\omega_0$. Next, correlating this information with the initial assumption we started with, i.e., $j\omega_0$ is the eigenvalue of the Hamiltonian matrix $\boldsymbol{M}$, we can infer that an imaginary eigenvalue of Hamiltonian matrix $\boldsymbol{M}$ corresponds to the frequency at which $\boldsymbol{F}(j\omega)$ is singular.

On the lines similar to the proof of the above theorem, the corollary of Theorem 3 (*Corollary*: The Hamiltonian matrix $\boldsymbol{M}$ has an eigenvalue $j\omega_0$, if the real part of the corresponding symmetric admittance matrix, $\boldsymbol{F}(j\omega)$ is singular at $j\omega_0$, provided $\boldsymbol{D}+\boldsymbol{D}^t$ is a positive-definite matrix) can also be proved.

REFERENCES

[1] R. Achar and M. Nakhla, "Simulation of high-speed interconnects," *Proc. IEEE*, vol. 89, pp. 693–728, May 2001.

[2] H. B. Bakoglu, *Circuits, Interconnections and Packaging for VLSI*. Reading, MA: Addison-Wesley, 1990.

[3] A. Deustsch, "Electrical characteristics of interconnections for high-performance systems," *Proc. IEEE*, vol. 86, pp. 315–355, Feb. 1998.

[4] C. Paul, *Analysis of Multiconductor Transmission Lines*. New York: Wiley, 1994.

[5] M. Nakhla and R. Achar, "Multimedia book series on signal integrity," Tech. Rep., OMNIZ Global Knowledge Corp., Ottawa, ON, Canada, http://www.omniz.com, 2002.

[6] L. M. Silveria, I. M. Elfadel, J. K. White, M. Chilukuri, and K. S. Kundert, "An efficient approach to transmission line simulation using measured or tabulated S-parameter data," in *Proc. ACM/IEEE Design Automat. Conf.*, June 1994, pp. 634–639.

[7] J. E. Schutt-Aine and R. Mittra, "Scattering parameter transient analysis of transmission lines loaded with nonlinear terminations," *IEEE Trans. Microwave Theory Tech.*, vol. 36, pp. 529–536, Mar. 1988.

[8] D. Winklestein, M. B. Steer, and R. Pomeerleau, "Simulation of arbitrary transmission line networks with nonlinear terminations," *IEEE Trans. Circuits Syst.*, vol. 38, pp. 418–422, Apr. 1991.

[9] W. T. Beyene and J. E. Schutt-Aine, "Accurate frequency-domain modeling and efficient simulation of high-speed packaging interconnects," *IEEE Trans. Microwave Theory Tech.*, vol. 45, pp. 1941–1947, Oct. 1997.

[10] M. Elzinga, K. L. Virga, L. Zhao, and J. L. Prince, "Pole-residue formulation for transient simulation of high-frequency interconnects using householder LS curve-fitting techniques," *IEEE Trans. Adv. Packag.*, vol. 25, pp. 142–147, May 2000.

[11] R. Achar, P. Gunupudi, M. Nakhla, and E. Chiprout, "Passive interconnect reduction algorithm for distributed/measured networks," *IEEE Trans. Computer-Aided Syst. II*, vol. 47, pp. 287–301, Apr. 2000.

[12] B. Gustavsen and A. Semlyen, "Rational approximation of frequency domain responses by vector fitting," *IEEE Trans. Power Delivery*, vol. 14, pp. 1052–1061, July 1999.

[13] R. Neumayer, F. Haslinger, A. Stelzer, and R. Weigel, "On the synthesis of equivalent circuit models for multiports characterized by frequency-dependent parameters," *IEEE Trans. Microwave Theory Tech.*, vol. 50, pp. 2789–2796, Dec. 2002.

[14] W. T. Beyene and J. E. Schutt-Aine, "Efficient transient simulation of high-speed interconnects characterized by sampled data," *IEEE Trans. Comp., Packag., Manufact. Technol. B*, vol. 21, pp. 105–114, Feb. 1998.

[15] ——, "Interconnect simulation using order reduction and scattering parameters," in *Proc. IEEE Electron. Comp. Technol. Conf.*, 1998, pp. 627–631.

[16] M. Elzinga, K. L. Virga, and J. L. Prince, "Improved global rational approximation macromodeling algorithm for networks characterized by frequency-sampled data," *IEEE Trans. Microwave Theory Tech.*, vol. 48, pp. 1461–1468, Sept. 2000.

[17] C. P. Coelho, J. R. Phillips, and L. M. Silveira, "Robust rational function approximation algorithm for model generation," in *Proc. 36th DAC*, New Orleans, LA, June 1999, pp. 207–212.

[18] J. Morsey and A. C. Cangellaris, "Passive realization of interconnect models from measured data," in *Proc. IEEE 10th Topical Meeting EPEP*, Cambridge, MA, Oct. 2001, pp. 47–50.

[19] S. Min and M. Swaminathan, "Efficient construction of two port passive macromodels for resonant networks," in *Proc. IEEE 10th Topical Meeting EPEP*, Cambridge, MA, Oct. 2001, pp. 230–232.

[20] C. P. Coelho, J. R. Phillips, and L. M. Silveira, "Passive constrained rational approximation algorithm using nevanlinna-pick interpolation," in *Proc. Design, Automatic Test Eur. Conf. Exhibition*, Mar. 2002, pp. 923–930.

[21] ——, "A convex programming approach to positive real rational approximation," in *Proc. IEEE/ACM Int. Conf. Computer-Aided Design*, Nov. 2001, pp. 245–251.

[22] D. Saraswat, R. Achar, and M. Nakhla, "A fast algorithm and practical considerations for passive macromodeling of measured/simulated data," in *Proc. IEEE 11th Topical Meeting Electric Performance in Electronic Packaging*, Monterey, CA, Oct. 2002, pp. 297–300.

[23] S. Lin and E. S. Kuh, "Transient simulation of lossy interconnects based on the recursive convolution formulation," *IEEE Trans. Circuits Syst.*, vol. 39, pp. 879–892, Nov. 1992.

[24] R. Achar and M. Nakhla, "Minimum realization of reduced-order models of high-speed interconnect macromodels," in *Signal Propagation on Interconnects*. Boston, MA: Kluwer, 1998, ch. III, pp. 23–45.

[25] K. J. Kerns and A. T. Yang, "Preservation of passivity during RLC network reduction via split congruence transformations," *IEEE Trans. Computer-Aided Design*, vol. 17, pp. 582–591, July 1998.

[26] A. Odabasioglu, M. Celik, and L. T. Pillage, "PRIMA: Passive reduced-order interconnect macromodeling algorithm," *IEEE Trans. Computer-Aided Design*, vol. 17, pp. 645–654, Aug. 1998.

[27] E. Kuh and R. Rohrer, *Theory of Active Linear Networks*. San Francisco, CA: Holden-Day, 1967.

[28] L. Weinberg, *Network Analysis and Synthesis*. New York: McGraw-Hill, 1962.

[29] B. Gustavsen and A. Semlyen, "Enforcing passivity for admittance matrices approximated by rational functions," *IEEE Trans. Power Syst.*, vol. 16, pp. 97–104, Feb. 2001.

[30] D. Saraswat, R. Achar, and M. Nakhla, "Passive macromodels of microwave subnetworks characterized by measured/simulated data," in *Int. Microwave Symp. Dig.*, Philadelphia, PA, June 2003, pp. 999–1002.

[31] ——, "On passivity check and compensation of macromodels from tabulated data," in *Proc.7th IEEE Workshop Signal Propagation and Interconnects*, Siena, Italy, May 2003, pp. 25–28.

[32] ——, "Enforcing passivity for rational function based macromodels of tabulated data," *IEEE Elect. Perform. Electron. Packag.*, pp. 295–298, Oct. 2003.

[33] M. E. Valkenburg, *Introduction to Modern Network Synthesis*. New York: Wiley, 1960.

[34] Y. Saad, *Iterative Methods for Sparse Linear Systems*. Boston, MA: PWS, 2000.

[35] T. Kailath, *Linear Systems*. Toronto, ON, Canada: Prentice-Hall, 1980.

[36] C. T. Chen, *Linear System Theory and Design*. New York: Holt, Rinehart and Winston, 1984.

[37] S. Boyd, L. El Ghaoui, E. Feron, and V. Balakrishnan, *Linear Matrix Inequalities in System and Control Theory*, Singapore: SIAM, Studies in Applied Mathematics, 1994, vol. 15.

[38] P. A. Parrilo, "Structured semidefinite programs and semi-algebraic geometry methods in robustness and optimization," Ph.D. dissertation, California Inst. Technol., Pasadena, CA, 2000.

[39] *Star-HSPICE Manual, Release 2001.2*, Synopsis Inc., Santa Clara, CA, 2001.

Dharmendra Saraswat (S'03) received the B.E. degree from the Goa Engineering College, Jabalpur, India, in 1990, and the M.A.Sc. degree from Carleton University, Ottawa, ON, Canada, in 2003 where he is currently pursuing the Ph.D. degree in electrical engineering.

His research interests include modeling and simulation of high-speed interconnect networks, circuit simulation and numerical algorithms.

Mr. Saraswat received the Natural Sciences and Engineering Research Council Scholarship, the 2002 Best Student Paper Award presented at the Electrical Performance of Electronic Packaging Conference, and the Third Best Student Paper Award presented at the International Microwave Symposium in 2003.

Ramachandra Achar (S'95–M'00) received the B.Eng. degree in electronics engineering from Bangalore University, Bangalore, India, in 1990, the M.Eng. degree in microelectronics from the Birla Institute of Technology and Science, Pilani, India, in 1992, and the Ph.D. degree from Carleton University, Ottawa, ON, Canada, in 1998.

He currently is an Assistant Professor in the Department of Electronics, Carleton University. He spent the Summer of 1995 working on high-speed interconnect analysis at the T. J. Watson Research Center, IBM, Yorktown Heights, NY. He was a Graduate Trainee at the Central Electronics Engineering Research Institute, Pilani, India, during 1992 and was also previously at Larsen and Toubro Engineers Ltd., Mysore, India, and at the Indian Institute of Science, Bangalore, India as an R&D Engineer. From 1998 to 2000, he was a Research Engineer in the CAE Group, Carleton University. His research interests include modeling and simulation of high-speed interconnects, model-order reduction, numerical algorithms, and development of computer-aided design tools for high-frequency circuit analysis.

Dr. Achar received the University Medal for his doctoral work on high-speed VLSI interconnect analysis, the Natural Science and Engineering Research Council (NSERC) doctoral award (2000), the Strategic Microelectronics Corporation (SMC) Award (1997), the Canadian Microelectronics Corporation (CMC) Award (1996), and the Best Student Paper Award at the 1998 Micronet (a Canadian Network of Centres of Excellence on Microelectronics) annual workshop.

Michel S. Nakhla (S'73–M'75–SM'88–F'98) received the M.A.Sc. and Ph.D. degrees in electrical engineering from the University of Waterloo, Waterloo, ON, Canada, in 1973 and 1975, respectively.

He is the Chancellor's Professor of Electrical Engineering at Carleton University, Ottawa, ON. From 1976 to 1988 he was with Bell-Northern Research, Ottawa, as the Senior Manager of the Computer-Aided Engineering Group. In 1988, he joined Carleton University as a Professor and the holder of the Computer-Aided Engineering Senior Industrial Chair (established by Bell-Northern Research and the Natural Sciences and Engineering Research Council of Canada). He is the founder of the high-speed CAD research group at Carleton University. He serves as technical consultant for several industrial organizations and is the principal investigator for several major sponsored research projects. His research interests include CAD of VLSI and microwave circuits, modeling and simulation of high-speed interconnects, nonlinear circuits, multidisciplinary optimization, thermal and electromagnetic emission analysis, MEMS, and neural networks.

Dr. Nakhla was a Guest Editor for the IEEE TRANSACTIONS ON ADVANCED PACKAGING and the IEEE TRANSACTIONS ON CIRCUITS AND SYSTEMS–PART II: ANALOG AND DIGITAL SIGNAL PROCESSING. He is currently Associate Editor of the IEEE TRANSACTIONS ON CIRCUITS AND SYSTEMS–PART I: FUNDAMENTAL THEORY and APPLICATIONS and Associate Editor of the *Circuits, Systems and Signal Processing Journal*.